

# Metal/dielectric thermal interfacial transport considering cross-interface electron-phonon coupling: Theory, two-temperature molecular dynamics, and thermal circuit

Zexi Lu, Yan Wang, and Xiulin Ruan\*

*School of Mechanical Engineering and the Birck Nanotechnology Center, Purdue University, West Lafayette, Indiana 47907, USA*

(Received 13 April 2015; revised manuscript received 23 November 2015; published 16 February 2016)

The standard two-temperature equations for electron-phonon coupled thermal transport across metal/nonmetal interfaces are modified to include the possible coupling between metal electrons with substrate phonons. The previous two-temperature molecular dynamics (TT-MD) approach is then extended to solve these equations numerically at the atomic scale, and the method is demonstrated using Cu/Si interface as an example. A key parameter in TT-MD is the nonlocal coupling distance of metal electrons and nonmetal phonons, and here we use two different approximations. The first is based on Overhauser's "joint-modes" concept, while we use an interfacial reconstruction region as the length scale of joint region rather than the phonon mean-free path as in Overhauser's original model. In this region, the metal electrons can couple to the joint phonon modes. The second approximation is the "phonon wavelength" concept where electrons couple to phonons nonlocally within the range of one phonon wavelength. Compared with the original TT-MD, including the cross-interface electron-phonon coupling can slightly reduce the total thermal boundary resistance. Whether the electron-phonon coupling within the metal block is nonlocal or not does not make an obvious difference in the heat transfer process. Based on the temperature profiles from TT-MD, we construct a new mixed series-parallel thermal circuit. We show that such a thermal circuit is essential for understanding metal/nonmetal interfacial transport, while calculating a single resistance without solving temperature profiles as done in most previous studies is generally incomplete. As a comparison, the simple series circuit that neglects the cross-interface electron-phonon coupling could overestimate the interfacial resistance, while the simple parallel circuit in the original Overhauser's model underestimates the total interfacial resistance.

DOI: [10.1103/PhysRevB.93.064302](https://doi.org/10.1103/PhysRevB.93.064302)

## I. INTRODUCTION

Modern electronic devices are aggressively shrinking into the nanoscale, and thermal transport at such scale is usually dominated by interfacial processes. Many methods have been applied to model nonmetal/nonmetal interfaces, including acoustic mismatch model (AMM) and diffuse mismatch model (DMM) [1], molecular dynamics [2,3], Green's function method [4,5], etc. On the other hand, many devices such as transistors [6,7] and heat-assisted magnetic recording (HAMR) devices [8] involve metal/dielectric or metal/semiconductor interfaces, and thermal transport in them is complicated by the role of electrons. In metals and dielectrics, electrons and phonons are the major thermal energy carriers, respectively [9]. Such carrier mismatch dictates electron-phonon energy redistribution to occur at the interfacial region. One useful approach to include electron-phonon coupling is the two-temperature model (TTM), where electrons and phonons are considered as two interacting subsystems [9,10]. It has been implemented into molecular dynamics (MD) and Boltzmann transport equations to model electron-phonon coupled thermal transport in metal/semiconductor systems [11–13]. Recently, we have employed two-temperature molecular dynamics (TT-MD) to predict interfacial thermal resistance of metal/nonmetal interfaces [14].

Experiments have demonstrated that at room temperature, the interfacial thermal conductances of several systems such as Pb/diamond and Au/diamond are much higher than the

values predicted by AMM or DMM models [15], indicating that mechanisms other than elastic phonon transmission are important. Several explanations have been proposed, but no consensus has been reached yet. One model, proposed by Overhauser [15], attributed the high interfacial thermal conductance to the coupling of metal electrons to the joint phonon modes formed at the interface. This mechanism is interesting and plausible, while the size of the joint-modes region was approximated as the phonon mean-free path without much justification. Also, it is questionable to treat the coupling of electrons with joint phonon modes as a single conductance channel without considering the phonon-phonon resistance inside the joint-modes region. Detailed discussions of these issues are provided in Sec. VB. Using the "joint-modes" concept, Sadasivam *et al.* performed first-principles calculations for the Eliashberg function of a heterojunction supercell to obtain a thermal conductance due to the coupling between electrons and joint phonon modes, and concluded that it cannot be neglected as compared to the phonon-phonon channel [16]. Sergeev proposed a Green's-function-based model to calculate the cross-interface coupling factor  $h_{ep}$  under a gray and diffusive assumption [17,18]. In contrast, several other studies have shown that this mechanism is not important at room temperature. Stoner and Maris applied time-domain thermal reflectance (TDTR) technique to measure the Kapitza conductance between metal/dielectric interfaces from 50 to 300 K, and claimed that the high conductance is not due to electronic effects but inelastic phonon process at the interface [19]. Cahill *et al.* used metals with very different electron density while keeping the other conditions similar, and observed similar interfacial thermal conductance, supporting the conclusion that electron-joint phonon modes

\*ruan@purdue.edu

coupling is insignificant [20,21]. Other experiments done by Hopkins *et al.* [22] came to the same conclusion. The existing TTM [9] and TT-MD [14] studies have also neglected cross-interface electron-phonon coupling. Such discrepancy warrants further theoretical and experimental investigation of the role of electrons. It should also be noted that when electrons in the metal are driven strongly out of equilibrium with the lattice, these high-energy electrons are at very high effective temperature ( $>4000$  K) and can indeed interact with phonons in the substrate directly [23–25]. Models such as the three-temperature model [24] have also been developed to include the cross-interface electron-phonon coupling mechanism for such highly nonequilibrium situations.

In this study we extend our previous TT-MD approach [14] by including the cross-interface electron-phonon coupling, in order to provide a simulation tool towards addressing the debate. We choose TT-MD since it can predict the temperature profiles and include all the potentially important process in a single simulation, including elastic and inelastic phonon scattering at the interface: electron-phonon coupling inside the metal as well as cross the interface. The goal of this work is to introduce the approach and the associated thermal circuit rather than to assess the relative importance of these processes that may well be system specific. The paper is organized as follows. First, modified two-temperature equations are introduced to allow the interaction of electrons in the metal with phonons in the dielectric. Then, TT-MD is developed to solve these equations numerically at the atomic scale, and the method is demonstrated using Cu/Si interface as the model system. Two different approximations are used to estimate the coupling distance between metal electrons and dielectric phonons. One is based on Overhauser’s “joint-modes” concept but with important modifications, and the other is based on a “phonon wavelength” concept. Later, the effects of including the cross-interface electron-phonon coupling on interfacial thermal resistance are discussed. Finally, a new thermal circuit is constructed based on the TT-MD results, and it is shown to be different from previous simple series or parallel thermal circuits. The new thermal circuit will provide essential insight towards resolving the debate.

## II. THEORY: MODIFIED TWO-TEMPERATURE EQUATIONS TO INCLUDE CROSS-INTERFACE ELECTRON-PHONON COUPLING

The standard two-temperature equations and the resulting temperature profiles of electrons and phonons across metal/nonmetal interfaces have been described in detail in Refs. [9,14], while the cross-interface electron-phonon coupling was not considered. However, the coupling of electrons in the metal with phonons in the dielectric is a possible thermal transport channel. Such cross-interface electron-phonon coupling is not well understood, and previous treatments by Sergeev [17,18] and Hopkins [24] are all based on the idea of electron interacting with a geometric interface without volume, which could be described by a Neumann boundary condition mathematically. However, recent studies indicated that this electron-ion interaction is a long-range effect [26]. Therefore, it is more reasonable to consider the cross-interface electron-phonon interaction as a volumetric effect.

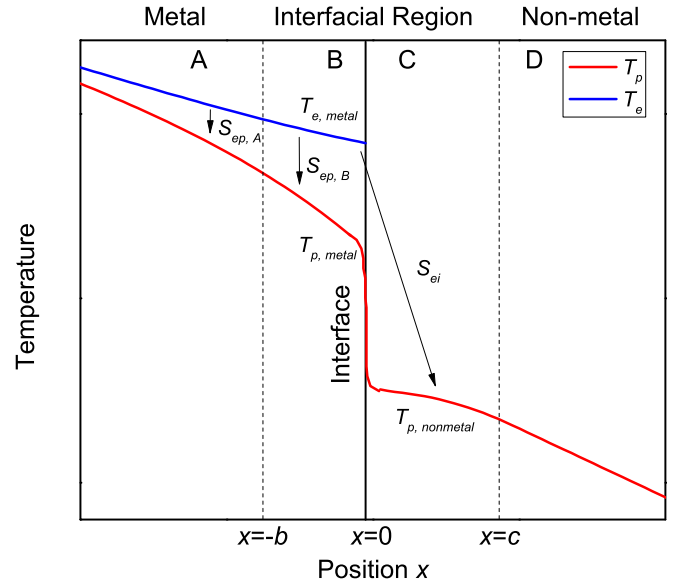


FIG. 1. The four regions defined at the metal/nonmetal interface in our analysis. Region A is the bulk metal region, while regions B and C are the interfacial regions, and region D is the bulk nonmetal region.

Here, we modify the standard two-temperature equations to include nonlocal electron-phonon coupling. Our model is illustrated in Fig. 1, in which the entire system is divided into four regions: A, B, C, and D. For simplicity, we still assume that the electron-phonon interaction is homogeneous in the metal, and the change of electron-phonon coupling strength near the boundary is ignored in the following analysis. Electrons in the nonmetal side are also ignored due to their negligible contribution [14,27]. The heat transfer process is considered in one-dimensional (1D) steady-state condition.

Region A is the part of metal that is far away from the interface, hence, the standard TTM governing equations could be applied:

When  $x < -b$ ,

$$k_{e,\text{metal}} \frac{\partial^2 T_{e,\text{metal}}}{\partial x^2} - S_{ep,A}(x) = 0, \quad (1a)$$

$$k_{p,\text{metal}} \frac{\partial^2 T_{p,\text{metal}}}{\partial x^2} + S_{ep,A}(x) = 0,$$

where  $k$  is the thermal conductivity of each carrier, and  $S_{ep,A}$  (unit:  $\text{W}/\text{m}^3$ ) is the internal volumetric heat generation due to electron-phonon coupling.

Region B is the near-interface part of the metal, where electrons in the metal can interact with phonons in both the metal (region B) and the nonmetal (region C). In other words, there are both bulk and cross-interface coupling for electrons in this region. The governing equations are

When  $-b < x < 0$ ,

$$k_{e,\text{metal}} \frac{\partial^2 T_{e,\text{metal}}}{\partial x^2} - S_{e,B}(x) = 0,$$

$$k_{p,\text{metal}} \frac{\partial^2 T_{p,\text{metal}}}{\partial x^2} + S_{ep,B}(x) = 0,$$

$$\begin{aligned}
S_{e,B}(x) &= S_{ep,B}(x) + S_{ei}(x), \\
S_{ep,B}(x) &= G_{ep,\text{metal}}[T_{e,\text{metal}}(x) - T_{p,\text{metal}}(x)], \\
S_{ei}(x) &= G_{ei}[T_{e,\text{metal}}(x) - T_{p,\text{nonmetal}}]. \quad (1b)
\end{aligned}$$

Here,  $G_{ep}$  and  $G_{ei}$  (unit:  $\text{W}/\text{m}^3\text{K}$ ) are the bulk electron-phonon coupling factor in the metal and the effective cross-interface electron-phonon coupling factor, respectively.  $S_{e,B}$  includes two parts: (1)  $S_{ep,B}$  is the volumetric heat generation due to bulk electron-phonon coupling, and (2)  $S_{ei}$  is the volumetric heat generation due to electrons in B interacting nonlocally with phonons in C. The last expression provides a method to estimate this amount.  $T_{p,\text{nonmetal}}$  is set as the average phonon temperature in region C. The choice of  $G_{ei}$  will be discussed in Sec. IV B.

In region C, no free electrons exist, but phonons can interact nonlocally with electrons in B. Therefore, the governing equation is

$$\begin{aligned}
\text{When } 0 < x < c, \\
k_{p,\text{nonmetal}} \frac{\partial^2 T_{p,\text{nonmetal}}}{\partial x^2} + S_{p,C}(x) &= 0, \quad (1c) \\
\int_{-b}^0 S_{ei}(x) dx &= \int_0^c S_{p,C}(x) dx,
\end{aligned}$$

where  $S_{p,C}$  is the volumetric energy source for phonons in the nonmetal, and its relation with  $S_{ei}$  is also expressed. Region D is the bulk part of nonmetal where heat is transferred by phonons, and the governing equation is

$$\begin{aligned}
\text{When } x > c, \\
k_{p,\text{nonmetal}} \frac{\partial^2 T_{p,\text{nonmetal}}}{\partial x^2} &= 0. \quad (1d)
\end{aligned}$$

So far, we have derived the governing equations for the metal/nonmetal interface. However, determining the size of regions B and C can be rather arbitrary due to the poor understanding of cross-interface electron-phonon coupling. Based on previous studies, here we use two approximations respectively. The first is based on the ‘‘joint-modes’’ concept proposed by Overhauser [15]. Although in their original model the size of the joint-modes region is the phonon mean-free path, here we modify it to the region of interfacial reconstruction according to our molecular dynamics results. The phonon spectrum in this region varies gradually from the bulk spectrum of one material to that of the other. This picture has been successfully used to gain more insights to phonon interfacial transport [28,29]. In our work, electrons in the metal side of the joint-modes region are assumed to interact with phonons in both sides of the joint-modes region. Therefore, regions B and C together in Fig. 1 are the joint-modes region, and the sizes can be predicted through MD simulations. It should be noted that the size will depend on the interfacial bonding strength. For example, van der Waals bonding leads to almost no joint-modes region [29]. The other approximation is the ‘‘phonon wavelength’’ model. Since phonon is a wave-particle dual description of lattice vibrations, it cannot be generated within a space that is smaller than its wavelength in any dimension. Meanwhile, we notice that the electron-phonon interaction is nonlocal since the Coulomb interaction between electrons and nuclei is long range. Therefore, each electron

is assumed to interact with phonons within a distance of the phonon wavelength on both left and right sides. In the interfacial region, electrons in the metal can interact with phonons in the nonmetal up to a distance of the average wavelength of the phonons in the nonmetal. Consequently, the electron-phonon coupling becomes nonlocal throughout the entire system.

### III. TT-MD SIMULATION APPROACH

We have previously employed TT-MD to numerically solve the standard two-temperature equations across metal/nonmetal interfaces [14]. Here, we modify the TT-MD approach to numerically solve the modified two-temperature equations described in the preceding section. The simulation system is divided into grids using finite volume method (FVM). Within a grid the atoms and the corresponding electrons interact with each other through the coupling term according to TTM theory.

To implement the joint-modes model to our original TT-MD, we assign a group of atoms, i.e., region C, in the nonmetal that will interact with electrons in the metal. The size of region C is determined by the size of the joint-modes region, which does not have a definite standard in the literature. In our model, it is defined as the region where the temperature profile becomes nonlinear in a nonequilibrium MD (NEMD) simulation, as used in several previous studies [28,29]. In a typical NEMD simulation [such as Figs. 4(a) and 4(b) in the later section], it is usually observed that the temperature profile becomes nonlinear near the interface of two dissimilar materials, which is due to interfacial reconstruction. The size of the reconstruction region is often affected by many factors such as the interfacial bonding strength, the cutoff range of the potentials used in the simulation, etc. In this study, the size of this nonlinear region is determined based on our MD simulations. At the interface, electrons in region B will have an additional interaction with phonons in region C, which is added to the FVM equation.

On the other hand, to implement the phonon wavelength model to our original TT-MD, the nonlocal electron-phonon interaction is applied throughout the entire system. Hence, the case is more complicated. In the FVM, electrons in each grid interact with phonons in the same grid as well as in adjacent grids within a distance of one phonon wavelength. This mechanism is illustrated in Fig. 2.

Each electron can couple to phonons in a region of  $2\lambda_{\text{avg}}$  centered on the electron. The bulk coupling strength is divided evenly into this region, so the overall effective coupling factor stays the same. We provide a more specific explanation of this by deriving a new expression for  $S_{ep,A}$  in Eq. (1a). For each electron located at  $x_0$ ,  $S_{ep,A}$  can be expressed as

$$S_{ep,A}(x_0) = \int_{x_0 - \lambda_{\text{avg}}}^{x_0 + \lambda_{\text{avg}}} \frac{G_{ep}}{2\lambda_{\text{avg}}} [T_e(x_0) - T_p(x)] dx. \quad (2)$$

The expression for  $S_{ep,B}$  is similar except that the upper limit in the integration has to be changed:

$$S_{ep,B}(x_0) = \int_{x_0 - \lambda_{\text{avg}}}^0 \frac{G_{ep}}{2\lambda_{\text{avg}}} [T_e(x_0) - T_p(x)] dx. \quad (3)$$

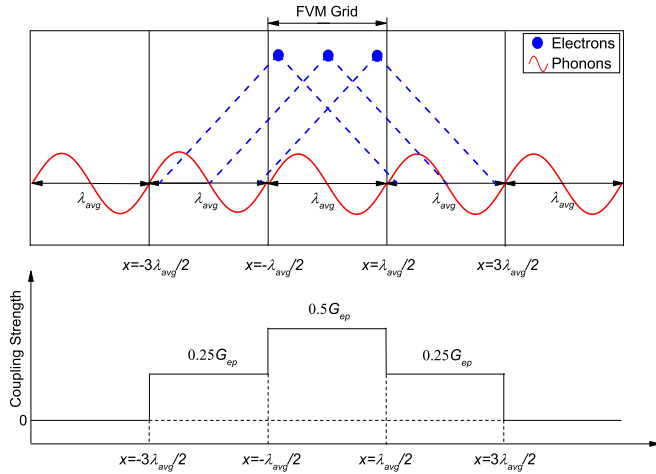


FIG. 2. Illustration of the nonlocal coupling mechanism. The system is discretized into grids using FVM.  $\lambda_{\text{avg}}$  is the average wavelength of phonons in the material. Each electron can couple to phonons in a region up to the length of  $2\lambda_{\text{avg}}$ . The upper figure also shows the coupling range of three different electrons: one in the center of the grid, and the other two near the boundary of the grid. The lower figure shows the effective coupling strength of electrons in the central grid to phonons from all the grids.  $G_{ep}$  is larger in the electrons' own grid, while smaller in the adjacent grids, and becomes zero in grids which are beyond the coupling range of any electron.

The size of region B is chosen as the same as that in the joint-modes model. In this way, the same amount of electrons are involved in the cross-interface electron-phonon coupling so that these two models are more comparable.

#### IV. Cu/Si CASE STUDY

In this section, we will present TT-MD simulation based on our models on the copper/silicon interface system.

##### A. Simulation system

The Cu/Si system we study here is the same as in our previous work [14], which is illustrated in Fig. 3. The system is set up initially with the periodic boundary condition in all three dimensions. Both Cu and Si are in contact via their (100) surface. The lattice parameters for Cu and Si are 3.61 and 5.43 Å, respectively, and the cross section of the system is  $10 \times 10$  Si unit cells or  $15 \times 15$  Cu unit cells. As a result, there is 0.3% mismatch between Cu and Si lattice in the cross-section plane. The length of the Si segment is 32 nm, while the length



FIG. 3. Illustration of the simulation system. Black parts refer to the fixed ends where atoms have no velocities. The red and blue parts are the heat source and heat sink, respectively. Heat flows in the direction perpendicular to the interface which results in 1D conduction. The periodic boundary condition is applied in the other two directions.

of the Cu segment is 96 nm. The many-body Tersoff potential [30] and the embedded-atom method (EAM) [31] potential are used for Si/Si and Cu/Cu interactions, respectively, and the interfacial Cu/Si interaction is described by the Morse potential [32]

$$U = D_e [e^{-2\alpha(r-r_0)} - 2e^{-\alpha(r-r_0)}], \quad (4)$$

where  $D_e = 0.9$  eV,  $\alpha = 1.11 \text{ \AA}^{-1}$ ,  $r_0 = 3.15 \text{ \AA}$ . Initially, the system is relaxed under zero-pressure using a Nose-Hoover thermostat [33] at 300 K for 0.3 ns, and then the fixed boundary condition is applied in the  $x$  direction in which the heat flows. A layer of two unit cells is fixed at each end. The atoms in these layers are set to zero velocity and zero force so there is no atomic interaction in these regions. The thickness of the two layers together is larger than the potentials' cutoff ranges. Therefore, the periodic boundary condition is transformed into the fixed boundary condition. Then, the system is switched to NEMD, where a constant heat flux of  $J = 3.2 \times 10^{-7}$  W is injected to the heat source region while extracted from the heat sink region, to establish 1D conduction. TTM calculation is presented on the Cu block included in this simulation domain. It is discretized into grids of 0.75 nm thickness for the FVM calculation. The size of the grid is approximately the same as the average phonon wavelength in Cu with a difference of 2%. Therefore, in the phonon wavelength model, electrons in each grid will interact with phonons in the same grid and also the two adjacent grids, just as illustrated in Fig. 2. However, it should be noted that we cannot specify the precise location of each electron or phonon within the grid, and not all the electrons and phonons in two adjacent grids can interact with each other (since the maximum distance between a pair of electron and phonon is  $2\lambda_{\text{avg}}$ , e.g., one phonon located at  $x = -3\lambda_{\text{avg}}/2$  cannot interact with one electron located at  $x = \lambda_{\text{avg}}/2$ ). Therefore, in order to correctly implement Eq. (2), we need to specify the effective coupling strength to account for the actual number of interacting energy carriers. As is shown in Fig. 2,  $G_{ep}$  in one grid is divided into three parts: a local effective  $0.5G_{ep}$  in the central grid itself, and a nonlocal effective  $0.25G_{ep}$  in each of the two adjacent grids. In this way, the simulation is fully consistent with Eq. (2). The overall effective  $G_{ei}$  in region C is set to the same in both models. From the simulation results we can acquire the temperature profiles of both electrons and phonons, and the thermal properties of them.

##### B. Input parameter

Different from the original MD, TT-MD requires an extra set of input parameters (see Table I), mostly the electronic parameters of the metal.  $k_e$  can be estimated using the

TABLE I. Important input thermal properties.

Property	Value
$C_e$	$5.26 \times 10^4 \text{ J/m}^3\text{K}$
$k_e$	401 W/mK
$G_{ep,Cu}$	$5.5 \times 10^{16} \text{ W/m}^3\text{K}$
$G_{ei}$	$5.5 \times 10^{16} \text{ W/m}^3\text{K}$

Wiedemann-Franz law from copper's electrical conductivity. We use 401 W/mK at 300 K [34] as the value for  $k_e$ . For volumetric heat capacity  $C_e$  and  $G_{ep}$  within copper, Lin has shown a comprehensive work on the thermal electronic parameters of different metals [35]. It is reported that  $C_e$  is almost linearly proportional to  $T_e$  when  $T_e$  is below 1000 K.  $G_{ep}$  has reported values ranging from  $5.5 \times 10^{16}$  W/m<sup>3</sup>K to  $2.6 \times 10^{17}$  W/m<sup>3</sup>K [34,35]. Here, we choose  $5.5 \times 10^{16}$  W/m<sup>3</sup>K to be consistent with our previous work.  $b$  is the size of region B and  $c$  is the size of region C. They are determined with respect to different models. In the joint-modes model, as stated previously, they are determined by the size of the interfacial reconstruction region observed in MD simulations. The linear parts of the temperature profile in the bulk region of the materials are extrapolated to the interface, and the region near the interface where the actual temperature profile deviates from the extrapolated line is designated as the interfacial reconstruction region. In this work, we find that  $b$  is approximately 0.5 nm and  $c$  is within the range of  $1 \sim 1.5$  nm. We notice that this contradicts the arguments from some previous works that copper, which is softer than silicon, is expected to have a larger interfacial atomic reconstruction region [36]. We attribute this result to the following explanation: although copper is softer than silicon, they have rather similar Young's modulus (117 GPa of copper compared with 130 GPa of silicon). Meanwhile the phonon mean-free path in silicon (which spans over  $0 \sim 10^6$  nm) is much larger than that in copper (which spans over  $1 \sim 50$  nm). As a result, one can expect that the atomic reconstruction, which breaks lattice periodicity and hinders phonon transport, has a more profound effect on the phonon transport in silicon. Therefore, we think that it is reasonable to observe a larger interfacial atomic reconstruction region in silicon. In the phonon wavelength model, the average phonon wavelength is approximated using  $\lambda_{\text{avg}} = hv/k_B T$ , where  $v$  is the average sound velocity in that material,  $h$  is the Planck constant, and  $T$  is the temperature. Bulk properties of the material, rather than interfacial properties, are used here for simplicity. In silicon  $\lambda_{\text{avg}}$  is calculated to be 1.4 nm, which is within the reported range in previous work [37] and chosen as the value for  $c$ . Therefore, for both models, we set  $b = 0.5$  nm and  $c = 1.4$  nm. This makes the electron-phonon coupling style the only difference between these two models. According to previous studies,  $G_{ei}$  can be relatively very small when electron temperature is around 300 K [23,24]. However, in copper there are only acoustic phonons while in silicon there are also optical phonons, and electrons have been reported to couple strongly to some of the optical phonon branches [6,38], therefore, we assume that  $G_{ei} = G_{ep,\text{metal}}$ . Combined with our choice of  $c$ , we can obtain an equivalent interfacial thermal conductance  $h_{es}$  [24] of 77 MW/m<sup>2</sup>K, which is comparable with the reported value of  $10 \sim 100$  MW/m<sup>2</sup>K for Au/Si interface at room temperature [24]. Since copper and gold have the same crystal structure and  $G_{ep}$  of the same order, we believe our assumption is qualitatively reasonable.

It should be noted that the choices of many parameters used in this simulation are based on simple assumptions since commonly accepted prediction methods for these parameters are still not available. These parameters include (1) the coupling distance of nonlocal electron-phonon coupling. In

the phonon wavelength model, we have used the average phonon wavelength estimated from  $\lambda_{\text{avg}} = hv/k_B T$  which is based on the Debye approximation, hence,  $\lambda_{\text{avg}}$  primarily represents acoustic phonons. There are certainly other options. For example, it has been pointed out that different phonon branches have different coupling strength to electrons. Hence, one may weigh the average phonon wavelength with respect to the coupling strength. (2) Distribution of nonlocal electron-phonon coupling strength: currently in both models we have distributed electron's (or phonon's) coupling strength evenly into its coupling distance. However, alternative distribution such as Gaussian or exponential may be more realistic since electrons should couple to phonons nearby more strongly than phonons that are farther away. (3) The value of  $G_{ei}$ , which is a key factor in determining how efficient the cross-interface electron-phonon coupling could be, is arbitrary in our simulations. Overall, although these parameters are approximate, our primary goal is to demonstrate our TT-MD approach, and later establish a thermal circuit that could correctly describe the interfacial thermal transfer channels. These input parameters can be refined when more sophisticated prediction methods become available in the future.

### C. Results

We first present the results of the joint-modes model. The temperature profile is shown in Fig. 4(a), in which electrons and phonons have a linear equilibrium curve in the middle of the metal block but become nonequilibrium near the interface. The linear equilibrium curve is extrapolated towards the interface. The total interfacial thermal resistance is calculated as  $R = \Delta T/J$ , where  $\Delta T$  is the temperature jump between  $T_{fit}|_{x=0}$  and  $T_p|_{x=0}$ . The total thermal boundary resistance (TBR) is calculated to be  $2.29 \times 10^{-9}$  m<sup>2</sup> K/W, which is about 18% lower than the TBR value of  $2.8 \times 10^{-9}$  m<sup>2</sup> K/W reported in our previous TT-MD model that did not consider the cross-interface electron-phonon coupling [14].

Then, we present the simulation results using the phonon wavelength model on the same system, where all the conditions and parameters applied are the same as the joint-modes model except the coupling style. The temperature profile is shown in Fig. 4(b). Generally with this global nonlocal coupling we would expect the results to be different from the joint-modes model. For instance, the electron-phonon nonequilibrium is expected to be smaller. However, the results turn out to be fairly similar. The total TBR is calculated to be  $2.33 \times 10^{-9}$  m<sup>2</sup> K/W, which is about 1.5% larger than that in the joint-modes model. The results of TBR from our original TT-MD in Ref. [14] and two new models in this work are listed in Table II.

## V. THERMAL CIRCUIT ANALYSIS

### A. Thermal circuit based on our models

If the cross-interface electron-phonon coupling is not considered, the thermal circuit is a simple series circuit of the electron-phonon and phonon-phonon coupling resistances [14]. It will be insightful to see how the thermal circuit should change after this effect is included. By adding an additional cross-interface electron-phonon coupling channel to

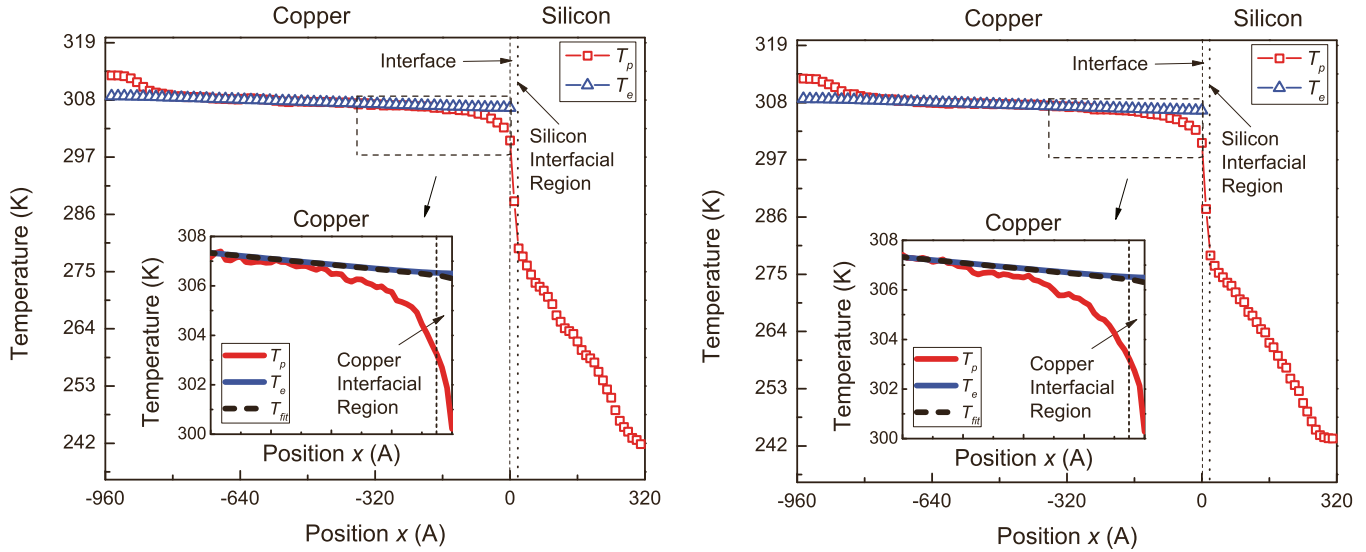


FIG. 4. (a) Temperature profile from a TT-MD simulation on the Cu/Si system with electron-phonon nonlocal coupling using the joint-modes model. The fitted temperature is acquired by extrapolation. It can be observed that the fitted temperature is almost identical to electrons' temperature since electrons have a much higher effective thermal conductivity. (b) Temperature profile from the phonon wavelength model. Overall, the result is not much different from that of the joint-modes model.

the original circuit [14], the thermal circuit can be established as shown in Fig. 5(b). Among these resistances,  $R_{pp}$  can be calculated based on the phonon temperature jump in the MD simulations.  $R_{ep,tot}$  is the electron-phonon coupling resistance in the metal which we divide into two parts:  $R_{ep,A}$  which is the electron-phonon coupling outside of the interfacial region but within the electron cooling length, and  $R_{ep,B}$  which is the electron-phonon coupling within the interfacial region. The energy transfer is marked as  $S_{ep,A}$  and  $S_{ep,B}$ , respectively. Since the size of region B is very small compared with the entire metal block,  $R_{ep,B}$  is approximated as

$$R_{ep,B} = \frac{1}{h_{ep,B}} = \frac{1}{G_{ep,B}b}, \quad (5)$$

where  $G_{ep,B}$  is assumed to be the same as in the bulk metal. Finally,  $R_{ei}$  can be fitted using the total TBR and all the other known resistances. The decomposed resistances are listed in Table III. Take the results from the phonon wavelength model as an example,  $R_{ep,tot}$  is  $0.60 \times 10^{-9}$  m<sup>2</sup> K/W, with  $R_{ep,A}$  being  $0.61 \times 10^{-9}$  m<sup>2</sup> K/W and  $R_{ep,B}$  being  $3.64 \times 10^{-8}$  m<sup>2</sup> K/W.  $R_{pp}$  is  $2.20 \times 10^{-9}$  m<sup>2</sup> K/W. Since the overall TBR is  $2.33 \times 10^{-9}$  m<sup>2</sup> K/W, we can obtain an  $R_{ei}$  of  $1.26 \times 10^{-8}$  m<sup>2</sup> K/W. The value is comparable with results of  $R_{ei,Au/Si} = 0.01 \sim 10 \times 10^{-8}$  m<sup>2</sup> K/W measured using TDTR in Refs. [24,25]. It is noteworthy that if we use Eq. (5) to estimate  $R_{ei}$  (rather than fitting) while we replace  $G_{ep,B}$  and  $b$  with  $G_{ei}$  and  $c$ , respectively, we obtain

a result of  $1.30 \times 10^{-8}$  m<sup>2</sup> K/W, which is pretty close to the fitted value with a difference of 3.2%.  $R_{ei}$  is much larger compared with other resistances, indicating that the cross-interface electron-phonon coupling is weaker than local coupling even when we assign the coupling factor to be the same. By decomposing the interfacial thermal resistance, our thermal circuit can be used exactly for evaluating the relative importance of the thermal conductance due to electron-phonon coupling. A larger electron-phonon coupling strength will decrease both resistances in the parallel channels in the thermal circuit, therefore increasing the interfacial conductance. The significance of this effect varies among systems and depends on material types, temperature, interface quality, etc.

## B. Merits and drawbacks of the original model of Huberman and Overhauser [15]

The concept of “joint phonon modes” at the interface was proposed by Huberman and Overhauser in Ref. [15], where the interface was understood as a joint region rather than an abrupt geometric interface. This concept was successfully used by several groups later to decompose the phonon interfacial resistance into interfacial region resistance and boundary resistance [28,29]. When using their model to treat electron-phonon coupled transport across an interface, however, we should note both the merits and drawbacks. In their model, which we designate as “Overhauser’s model,” the “joint-modes” region extends to one phonon mean-free path on each side of the interface. Therefore, the material with longer phonon mean-free path will have larger portion of the joint-modes region. In the joint-modes region, the atoms are at a uniform temperature and vibrate in the same “joint modes.” Under Overhauser’s model, the corresponding temperature profile is shown in Fig. 5(c), where the temperature of the joint-modes region is uniform and equal to the temperature of the silicon side due to much longer phonon mean-free path in silicon than in copper. As a result, the

TABLE II. Results of TBR from different MD simulations.

Model	$R_{Bd,tot}$ (m <sup>2</sup> K/W)
Original TT-MD	$2.8 \times 10^{-9}$
The joint-modes model	$2.29 \times 10^{-9}$
The phonon wavelength model	$2.33 \times 10^{-9}$

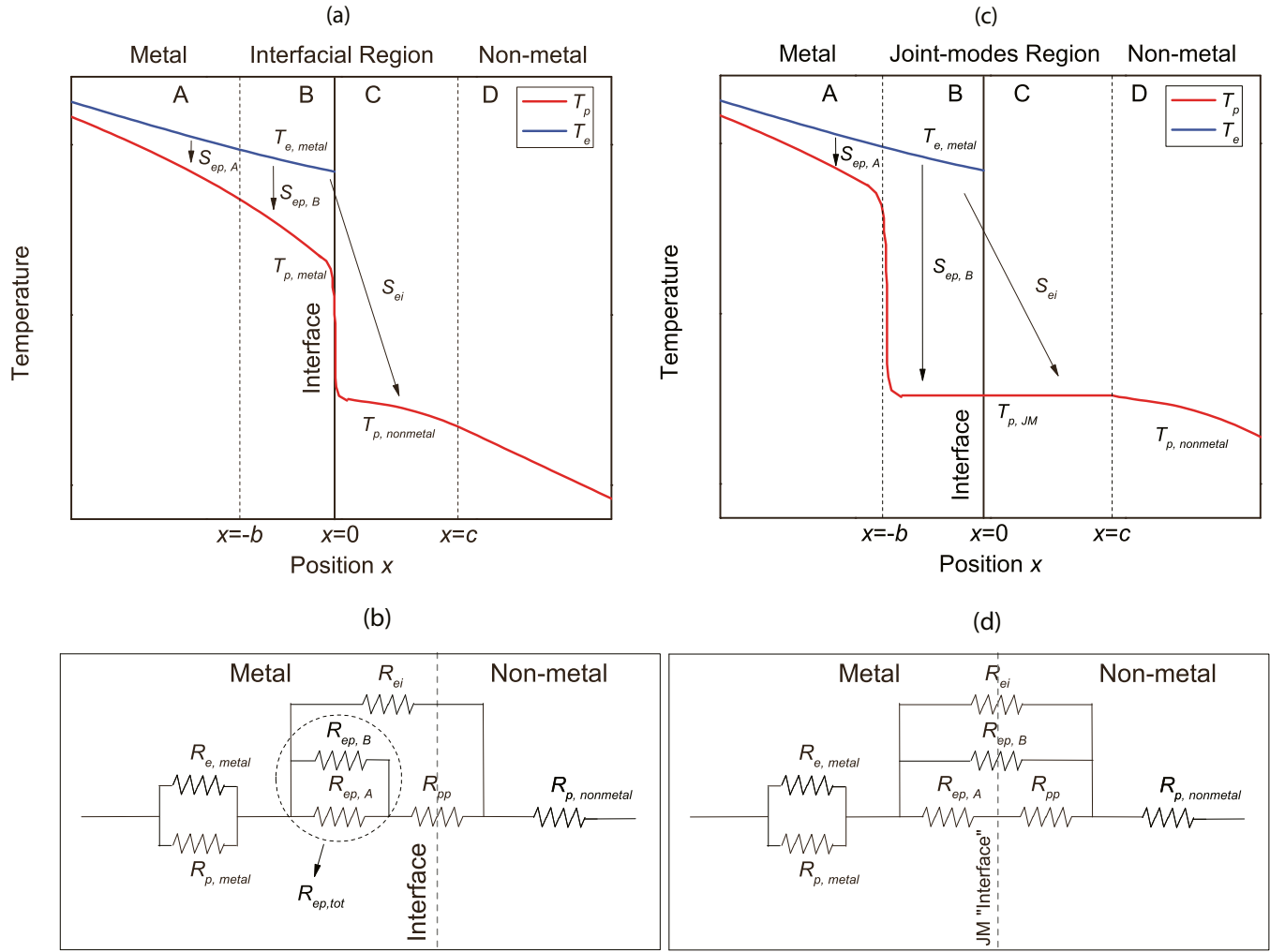


FIG. 5. (a), (b) Qualitative temperature profile of our model and the corresponding thermal circuit. (c), (d) Qualitative temperature profile of Overhauser's model and the corresponding thermal circuit.  $R_{ep,tot}$  is the resistance due to electron-phonon nonequilibrium,  $R_{pp}$  is the resistance due to phonon-phonon cross-interface coupling, and  $R_{ei}$  represents the channel of electron-phonon cross-interface coupling.

temperature jump has to occur in copper somewhere outside of the joint-modes region. Under this picture, the electron-phonon energy transfer in the metal side of the joint-modes region ( $S_{ep,B}$ ) becomes an independent conductance channel. The corresponding thermal circuit is depicted in Fig. 5(d). Applying this model to our system, then the sizes of regions B and C are modified to be  $b = 4.1$  nm and  $c = 30$  nm, which are the approximate average phonon mean-free paths in copper

TABLE III. Results of decomposed TBR in different models (values are in unit of  $m^2$  K/W).

Resistances	Our models		Overhauser's model
	Joint-modes model	Phonon wavelength model	
$R_{Bd,tot}$	$2.29 \times 10^{-9}$	$2.32 \times 10^{-9}$	$4.50 \times 10^{-10}$
$R_{pp}$	$2.20 \times 10^{-9}$	$2.20 \times 10^{-9}$	$2.20 \times 10^{-9}$
$R_{ep,A}$	$0.61 \times 10^{-9}$	$0.61 \times 10^{-9}$	$0.69 \times 10^{-9}$
$R_{ep,B}$	$3.64 \times 10^{-8}$	$3.64 \times 10^{-8}$	$4.43 \times 10^{-9}$
$R_{ei}$	$1.26 \times 10^{-8}$	$1.35 \times 10^{-8}$	$6.06 \times 10^{-10}$

and silicon, respectively. In determining the values of each individual resistance,  $R_{e,metal}$  and  $R_{p,metal}$  are assumed to be the same because the size difference of region B only changes these values by less than 1%.  $R_{pp}$  is also set as the average of the results predicted by our MD simulations.  $R_{ep,tot}$  is broken down in the same way as previously, and  $R_{ep,B}$  is determined by Eq. (5) as well.  $R_{ei}$  is also determined using Eq. (5), but  $G_{ep,B}$  is replaced with  $G_{ei}$  and  $b$  is replaced with  $c$ . The results are listed in the last column of Table III. It turns out that the total TBR predicted by their model is only 20% of the value of our model. We attribute the difference to two reasons. First, our TT-MD simulation results in Fig. 4 show that the phonon temperature in the joint-modes region rapidly drops rather than being uniform. Similar results have been obtained in other previous works [28,29]. This is reasonable since the joint-modes region is the location where most mismatch occurs, and the temperature drop should occur here rather than in the homogeneous metal outside of the joint-modes region. We consider the assumption of uniform temperature in the joint-modes region in Overhauser's model unphysical. As a result, the electron-phonon coupling in the metal side of the joint-modes region ( $R_{ep,B}$ ) is in series with the phonon-phonon coupling across the

interface  $R_{pp}$ , rather than being an independent conductance channel. The accurate thermal circuit should be represented by Fig. 5(b) instead of 5(d). Therefore, knowing the temperature profiles and then constructing the correct thermal circuit is essential for any prediction of the metal/dielectric interfacial transport. Second, the size of the joint-modes region is different between our model and Overhauser's model. To determine the value of  $R_{ei}$  in Overhauser's model, the effective phonon mean-free path is used and it is assumed that electrons in B can couple evenly to phonons in C, and the relatively large size of region C leads to a very small  $R_{ei}$  compared with other resistances. In fact, a choice of  $c = 30$  nm is already conservative since the spectral phonon mean-free path in silicon can span several orders of magnitude [39]. However, since electrons lose energy primarily to optical phonons, it will be more appropriate to consider optical phonon mean-free path which is usually much smaller than the effective phonon mean-free path. Indeed, recent MD simulations have indicated that the joint-modes region is small, on the scale of phonon wavelength or several bond lengths [28,29]. Nevertheless, the impact range of nonlocal electron-phonon coupling is not well understood yet and deserves further studies. In Overhauser's original model, these two factors have contributed to the overestimation of the contribution of cross-interface electron-phonon coupling to the interfacial thermal conductance.

## VI. SUMMARY

We have presented a TT-MD framework to simulate electron-phonon thermal transport across metal/nonmetal

interfaces, which includes the nonlocal electron-phonon coupling effect. We have extended the previous TT-MD model and proposed two new models with different coupling mechanism to interpret the process: the "joint-modes" model and the "phonon wavelength" model. By conducting simulations on the Cu/Si interface which are comparable with the previous study, we obtain results indicating that the proposed mechanism can slightly enhance interfacial thermal transport. The total TBR is reduced by 18% if the cross-interface electron-phonon coupling is considered. Based on the TT-MD results, we construct a mixed series-parallel thermal circuit, where the electron-phonon coupling resistance in the metal side of the interfacial region is in series with the phonon-phonon resistance, and they together are in parallel with the electron-phonon coupling resistance in the dielectric side of the interfacial region. As a comparison, the simple series circuit that neglects the cross-interface electron-phonon coupling slightly overestimates the interfacial resistance, while the simple parallel circuit under the Overhauser picture underestimates the total interfacial resistance. Knowing electron and phonon temperature profiles and the corresponding thermal circuit is essential to understand metal/dielectric interfacial transport.

## ACKNOWLEDGMENTS

The authors thank the support from the Air Force Office of Scientific Research (AFOSR). We also thank Sridhar Sadasivam and Prof. Timothy Fisher for fruitful discussions.

- 
- [1] E. Swartz and R. Pohl, *Rev. Mod. Phys.* **61**, 605 (1989).
  - [2] R. J. Stevens, L. V. Zhigilei, and P. M. Norris, *Int. J. Heat Mass Transfer* **50**, 3977 (2007).
  - [3] E. S. Landry and A. J. H. McGaughey, *Phys. Rev. B* **80**, 165304 (2009).
  - [4] W. Zhang, T. S. Fisher, and N. Mingo, *J. Heat Transfer* **129**, 483 (2006).
  - [5] Z. Huang, T. S. Fisher, and J. Y. Murthy, *J. Appl. Phys.* **108**, 114310 (2010).
  - [6] J. A. Rowlette and K. E. Goodson, *IEEE Trans. Electron Devices* **55**, 220 (2008).
  - [7] J. Robertson, *Rep. Prog. Phys.* **69**, 327 (2005).
  - [8] L. Pan and D. B. Bogy, *Nat. Photonics* **3**, 189 (2009).
  - [9] A. Majumdar and P. Reddy, *Appl. Phys. Lett.* **84**, 4768 (2004).
  - [10] L. Koči, E. M. Bringa, D. S. Ivanov, J. Hawreliak, J. McNaney, A. Higginbotham, L. V. Zhigilei, A. B. Belonoshko, B. A. Remington, and R. Ahuja, *Phys. Rev. B* **74**, 012101 (2006).
  - [11] D. S. Ivanov and L. V. Zhigilei, *Phys. Rev. B* **68**, 064114 (2003).
  - [12] D. M. Duffy and A. M. Rutherford, *J. Phys.: Condens. Matter* **19**, 016207 (2007).
  - [13] Y. Wang, Z. Lu, A. K. Roy, and X. Ruan, *J. Appl. Phys.* **119**, 065103 (2016).
  - [14] Y. Wang, X. Ruan, and A. K. Roy, *Phys. Rev. B* **85**, 205311 (2012).
  - [15] M. L. Huberman and A. W. Overhauser, *Phys. Rev. B* **50**, 2865 (1994).
  - [16] S. Sadasivam, U. V. Waghmare, and T. S. Fisher, *J. Appl. Phys.* **117**, 134502 (2015).
  - [17] A. V. Sergeev, *Phys. Rev. B* **58**, R10199 (1998).
  - [18] A. Sergeev, *Physica B: Condens. Matter* **263-264**, 217 (1999).
  - [19] R. J. Stoner and H. J. Maris, *Phys. Rev. B* **48**, 16373 (1993).
  - [20] H.-K. Lyeo and D. G. Cahill, *Phys. Rev. B* **73**, 144301 (2006).
  - [21] G. T. Hohensee, R. B. Wilson, and D. G. Cahill, *Nat. Commun.* **6**, 6578 (2015).
  - [22] A. Giri, J. T. Gaskins, B. F. Donovan, C. Szejewski, R. J. Warzoha, M. A. Rodriguez, J. Ihlefeld, and P. E. Hopkins, *J. Appl. Phys.* **117**, 105105 (2015).
  - [23] P. E. Hopkins and P. M. Norris, *Appl. Surf. Sci.* **253**, 6289 (2007).
  - [24] P. E. Hopkins, J. L. Kassebaum, and P. M. Norris, *J. Appl. Phys.* **105**, 023710 (2009).
  - [25] L. Guo, S. L. Hodson, T. S. Fisher, and X. Xu, *J. Heat Transfer* **134**, 042402 (2012).
  - [26] N. Driza, S. Blanco-Canosa, M. Bakr, S. Soltan, M. Khalid, L. Mustafa, K. Kawashima, G. Christiani, H.-U. Habermeier, G. Khaliullin, C. Ulrich, M. Le Tacon, and B. Keimer, *Nat. Mater.* **11**, 675 (2012).
  - [27] R. E. Jones, J. A. Templeton, G. J. Wagner, D. Olmsted, and N. A. Modine, *Int. J. Numer. Methods Eng.* **83**, 940 (2010).
  - [28] S. Shin, M. Kaviani, T. Desai, and R. Bonner, *Phys. Rev. B* **82**, 081302 (2010).

- [29] J. Shi, Y. Dong, T. Fisher, and X. Ruan, *J. Appl. Phys.* **118**, 044302 (2015).
- [30] J. Tersoff, *Phys. Rev. B* **37**, 6991 (1988).
- [31] S. M. Foiles, M. I. Baskes, and M. S. Daw, *Phys. Rev. B* **33**, 7983 (1986).
- [32] S.-F. Hwang, Y.-H. Li, and Z.-H. Hong, *Comput. Mater. Sci.* **56**, 85 (2012).
- [33] S. Noseé, *J. Chem. Phys.* **81**, 511 (1984).
- [34] G. L. Eesley, *Phys. Rev. B* **33**, 2144 (1986).
- [35] Z. Lin, L. V. Zhigilei, and V. Celli, *Phys. Rev. B* **77**, 075133 (2008).
- [36] F. Sun, T. Zhang, M. M. Jobbins, Z. Guo, X. Zhang, Z. Zheng, D. Tang, S. Ptasinska, and T. Luo, *Adv. Mater.* **26**, 6093 (2014).
- [37] C. Dames, *J. Appl. Phys.* **95**, 682 (2004).
- [38] E. Pop, R. W. Dutton, and K. E. Goodson, *J. Appl. Phys.* **96**, 4998 (2004).
- [39] T. Feng and X. Ruan, *J. Nanomater.* **2014**, 206370 (2014).